ADVANCED ENERGY MATERIALS
www.advenergymat.de

Improved Cu_2O-Based Solar Cells Using Atomic Layer Deposition to Control the Cu Oxidation State at the p-n Junction

Sang Woon Lee, Yun Seog Lee, Jaeyeong Heo, Sin Cheng Siah, Danny Chua, Riley E. Brandt, Sang Bok Kim, Jonathan P. Mailoa, Tonio Buonassisi, and Roy G. Gordon**

Recombination at a defect-rich interface is one of the major efficiency-loss mechanisms in polycrystalline heterojunction thin-film solar cells.[1,2] Cuprous oxide (Cu_2O) is considered a promising Earth-abundant semiconductor for thin-film solar cells compatible with terawatt-level deployment.[3–5] However, the power conversion efficiency (PCE) of Cu_2O-based solar cells has remained significantly lower than the theoretical single-junction maximum efficiency of >20%, often due to low open-circuit voltages (V_{OC}) resulting from rapid interfacial recombination.[6–8] This interfacial recombination is believed to originate mostly from i) non-ideal band-alignment with an adjacent n-type transparent conductive oxide (TCO) layer (e.g., Al-doped ZnO or indium-tin-oxide) and ii) a high density of trap states in the region near the heterojunction interface. Various buffer layers including Ga_2O_3, TiO_2, and amorphous zinc-tin-oxide (a-ZTO) have been applied at the junction interface to provide more ideal band alignment.[6,9,10]

To reduce the interfacial trap density and further enhance heterojunction quality, any defects at the heterojunction interface should be minimized.[11] In particular, a cupric oxide (CuO) layer on the Cu_2O surface is highly undesirable since it has a smaller bandgap ($E_g \approx 1.4$ eV) than Cu_2O ($E_g \approx 2$ eV) and its conduction band energy near 4 eV from the vacuum level can create deep states at the interface, enhancing interfacial recombination.[3,12–14] A CuO layer is formed readily on a Cu_2O or Cu surface during quenching and/or exposure to an oxygen-rich ambient.[7,15] Similar surface chemistry changes are common for many thin-film solar cell materials including copper indium gallium selenide (CIGS).[16] In the past, chemical treatments have been employed to modify the surface chemistry of air-exposed CIGS films.[16,17] For Cu_2O prepared by a thermal oxidation method, similar methods for Cu_2O surface modification, including wet etching, heat treatments, and a catalyst layer, have been introduced to remove the CuO surface layers, resulting in enhancements of solar cell performance.[5,7,18] However, even if the surface treatments remove the CuO layer completely, a nanometer-scale-thick CuO layer can re-grow when the surface is exposed to air thereafter.[15] Thus, a surface modification process with high controllability should be performed in situ immediately prior to overlayer deposition during solar cell fabrication (e.g., buffer layer deposition) to achieve higher PCE. Recently, Wilson et al. proposed a method to control interface stoichiometry of Cu_2O in situ by controlling the oxygen partial pressure during sputtering of a ZnO over-layer.[14]

Here, we demonstrate a method to tune the chemical state of the interfacial layer of Cu_2O absorbers by chemical means, by engineering the atomic layer deposition (ALD) reaction conditions of an a-ZTO buffer layer in an all-oxide thin-film solar cell device architecture (ZnO:Al/a-ZTO/Cu_2O). During the past decade, ALD has demonstrated utility in a range of photovoltaic device-processing applications, including buffer-layer deposition and surface passivation.[19,20] The discrete nature of the ALD process enables a high degree of tunability of the layer properties as well as an excellent uniformity over large-scale substrates.[19–21]

We exploit the fact that ALD can involve highly reactive metal-precursors and oxidizers, which can also affect surface chemistry of substrates. We utilize the thermodynamics of the half-cycle reaction in the ALD sequence of a-ZTO buffer layer deposition to control the surface chemistry of as-grown Cu_2O thin-film, and describe how this approach could be generalized to other buffer-layer materials. The CuO (Cu^{2+} state) interfacial layer at a-ZTO/Cu_2O can be reduced to Cu_2O (Cu^{1+} state) by pulsing a Zn precursor, and additional oxidation of Cu_2O surface by an oxidant pulse can be suppressed by lowering the ALD reaction temperature. By engineering the surface chemistry associated with the ALD reaction temperature, the chemical state of Cu at the interface can be controlled and a high-quality heterojunction can be formed. We demonstrate the

Dr. S. W. Lee,[+] D. Chua, Dr. S. B. Kim, Prof. R. G. Gordon
Department of Chemistry and Chemical Biology
Harvard University
Cambridge, MA 02138, USA
E-mail: gordon@chemistry.harvard.edu
Dr. Y. S. Lee, S. C. Siah, R. E. Brandt, J. P. Mailoa, Prof. T. Buonassisi
Massachusetts Institute of Technology
Cambridge, MA 02139, USA
E-mail: buonassisi@mit.edu
Prof. J. Heo
Department of Materials Science and Engineering
Chonnam National University
Gwangju 500–757, Korea
[+]Present address: Department of Physics and Division of Energy Systems Research, Ajou University, Suwon 443–749, Korea

DOI: 10.1002/aenm.201301916

 © 2014 WILEY-VCH Verlag GmbH & Co. KGaA, Weinheim

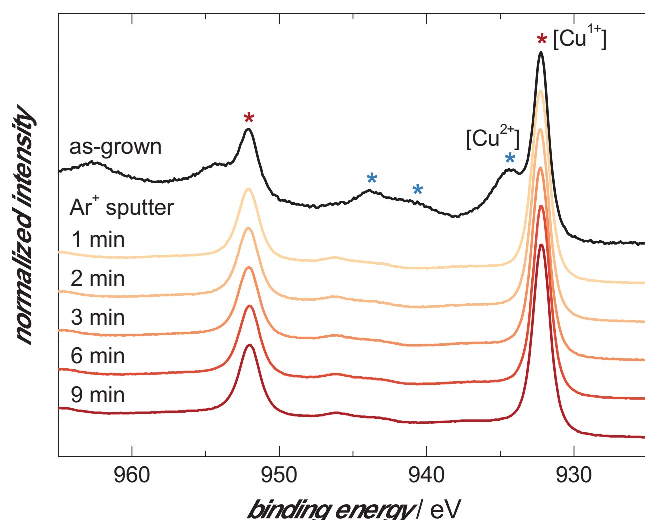

Figure 1. XPS spectra of Cu-2p core levels for an as-grown Cu_2O film surface and sputtered surfaces by Ar-ion at 1 keV in situ. The peaks from Cu^{1+} and Cu^{2+} states are shown in red and blue asterisks, respectively. The native CuO surface layer, which is removed by sputtering, is estimated to be 1 nm thin.

enhanced performance of Cu_2O-based solar cells by controlling interface chemistry, resulting in an improved V_{OC}.

A nanometer-scale-thick surface layer of CuO phase is normally formed on Cu_2O films grown by electrochemical deposition. **Figure 1** shows XPS spectra of the Cu-2p core levels for an as-grown Cu_2O film surface and a Cu_2O surface sputtered by argon ions at 1 keV in situ. Peaks at 932.2 and 934.2 eV indicate Cu^{1+} and Cu^{2+} states, respectively.[22,23] Broad satellite peaks near 940–945 eV originate from the CuO phase, which is a characteristic of materials having a d^9 configuration in the ground state.[23] Thus, the existence of the satellite peaks is an evidence of formation of the CuO phase in addition to the peak assigned to the Cu^{2+} state at ≈934 eV. After sputtering the sample surface for 1 min, the signals from the CuO phase disappear and only signals from the Cu_2O phase are observed. The XPS spectra with depth profiling suggest that the CuO forms only at the near-surface region of the Cu_2O. The CuO is likely due to exposure of the sample to ambient atmosphere, in which an abundance of oxygen can promote the complete oxidation of copper cations to Cu^{2+} (CuO).[23,24] Considering the electron escape depth of ≈5 nm and the XPS signal intensity of CuO phase relative to Cu_2O phase, the surface CuO layer is expected to have an approximate thickness of only 1 nm, perhaps suggesting that the formation of a thicker surface layer is limited by oxygen diffusion through CuO.

To remove the surface CuO layer and create a high-quality a-ZTO/Cu_2O interface, the thermodynamics of the a-ZTO ALD reaction are investigated. The optimized a-ZTO ALD consists of ZnO and SnO_2 deposition reactions with a pulse ratio of 3:1.[9,25] The starting sequence is a pulse of diethylzinc (DEZ) as a Zn precursor, followed by a pulse of hydrogen peroxide (H_2O_2) as an oxidizer. It has been reported that the injection of ALD metal precursors can reduce an underlying layer if the reactions are energetically favorable.[26,27] The Gibbs free energy of reaction (ΔG_r) can predict whether the surface reactions in a-ZTO ALD are spontaneous. Plausible reactions of DEZ with CuO and their ΔG_r at 373 K are the following:[28]

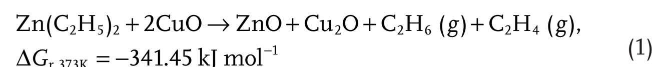

$$Zn(C_2H_5)_2 + 2CuO \rightarrow ZnO + Cu_2O + C_2H_6\,(g) + C_2H_4\,(g),\quad \Delta G_{r,373K} = -341.45\ \text{kJ mol}^{-1} \tag{1}$$

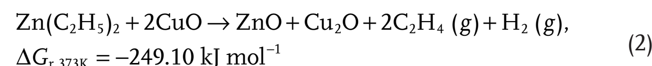

$$Zn(C_2H_5)_2 + 2CuO \rightarrow ZnO + Cu_2O + 2C_2H_4\,(g) + H_2\,(g),\quad \Delta G_{r,373K} = -249.10\ \text{kJ mol}^{-1} \tag{2}$$

or

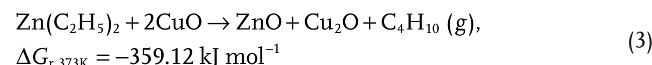

$$Zn(C_2H_5)_2 + 2CuO \rightarrow ZnO + Cu_2O + C_4H_{10}\,(g),\quad \Delta G_{r,373K} = -359.12\ \text{kJ mol}^{-1} \tag{3}$$

In addition, the reduction of Cu_2O to metallic Cu by DEZ is also possible by the following reactions:

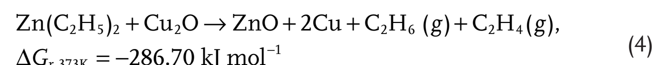

$$Zn(C_2H_5)_2 + Cu_2O \rightarrow ZnO + 2Cu + C_2H_6\,(g) + C_2H_4(g),\quad \Delta G_{r,373K} = -286.70\ \text{kJ mol}^{-1} \tag{4}$$

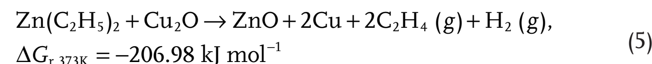

$$Zn(C_2H_5)_2 + Cu_2O \rightarrow ZnO + 2Cu + 2C_2H_4\,(g) + H_2\,(g),\quad \Delta G_{r,373K} = -206.98\ \text{kJ mol}^{-1} \tag{5}$$

or

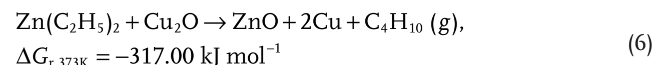

$$Zn(C_2H_5)_2 + Cu_2O \rightarrow ZnO + 2Cu + C_4H_{10}\,(g),\quad \Delta G_{r,373K} = -317.00\ \text{kJ mol}^{-1} \tag{6}$$

On the other hand, the H_2O_2 sequence after the DEZ pulse can oxidize Cu_2O to CuO by the following reaction:

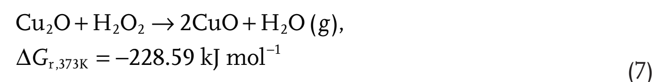

$$Cu_2O + H_2O_2 \rightarrow 2CuO + H_2O\,(g),\quad \Delta G_{r,373K} = -228.59\ \text{kJ mol}^{-1} \tag{7}$$

All reactions have negative ΔG_r at 373 K, indicating that both reduction and oxidation reactions are thermodynamically favorable in the presence of reducing and oxidizing precursors, respectively.

As the thermodynamic analysis predicts, the Zn precursor in the a-ZTO ALD process is experimentally observed to reduce the CuO surface layer to Cu_2O. **Figure 2**a shows normalized XPS spectra of Cu-2p at the Cu_2O surface after DEZ and an Sn(II) precursor (1,3-bis(1,1-dimethylethyl)-4,5-dimethyl-(4R,5R)-1,3,2-diazastannolidin-2-ylidene) were pulsed on Cu_2O films with CuO surface layers. Here, nine super-cycles (three DEZ pulses and one Sn(II) precursor pulse per one super-cycle) of metal precursor injections were used, skipping the injection of H_2O_2. Two reaction temperatures of 90 and 170 °C were investigated. At both temperatures, the intensities of the CuO peaks decreased after the injection of metal precursors, which indicates that the CuO layer was partially reduced to Cu_2O or Cu. The similar decrease in the intensity of the CuO peak for both temperatures suggests that the reduction rate is rapid at both temperatures. A control experiment was performed (the Cu_2O samples were kept in the chamber without doing any ALD treatment), which showed negligible change of XPS spectra as shown in Figure S1 (Supporting Information).

© 2014 WILEY-VCH Verlag GmbH & Co. KGaA, Weinheim

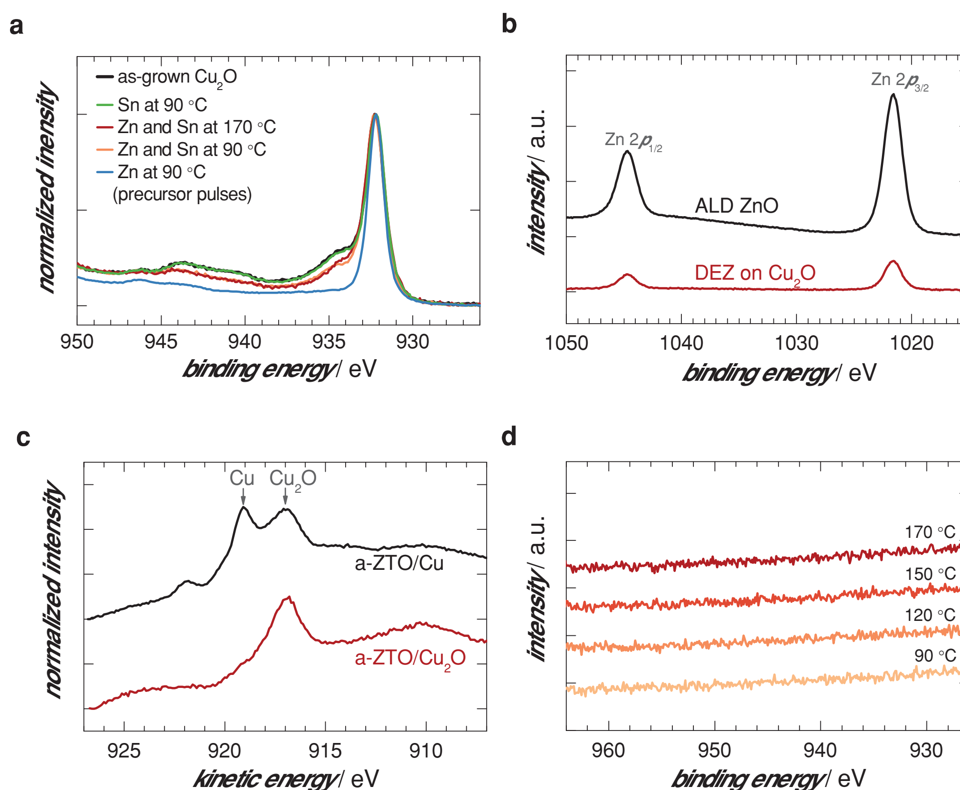

Figure 2. The Zn precursor in the a-ZTO ALD process is experimentally observed to reduce the oxidation state of the Cu_2O absorber's native CuO surface layer to Cu_2O. a) Normalized XPS spectra of Cu-2p of Cu_2O surface after a pulse of DEZ and Sn(II) molecules on electrochemically deposited Cu_2O films having nanometer-scale-thick CuO surface layers. b) XPS spectrum of Zn-2p core levels after a pulse of only DEZ molecules on a Cu_2O film at 90 °C, showing the same Zn-2p core levels as a ZnO film grown by ALD using DEZ and H_2O_2. c) The Cu-LMM Auger spectra from Cu_2O and metallic Cu after the growth of a-ZTO layer by ALD at 90 °C. 20-nm-thick Cu film was prepared by e-beam evaporation at room temperature for the comparison. d) XPS spectra of Cu-2p core levels with 10-nm-thick a-ZTO films deposited on Cu_2O at reaction temperatures between 90 and 170 °C, showing no signal from elemental Cu for all temperatures, which indicates no Cu diffusion occurred.

When only Sn(II) precursor pulses were introduced to the Cu_2O film while not injecting DEZ or H_2O_2 with the same conditions mentioned above, negligible reduction of the CuO layer was observed. In contrast, the injection of DEZ without any Sn(II) precursor or H_2O_2 significantly decreased the intensity of the CuO peak. Thus, the reduction of the CuO layer is mainly driven by DEZ, forming a stable ZnO without the aid of the oxidant (Figure 2b). The reduction of Cu_2O by the Sn(II) precursor is thermodynamically or kinetically unfavorable. Interestingly, the reduction of CuO is most effective when only DEZ was introduced without any Sn(II) precursor, which suggests the surface-adsorbed Sn(II) precursor inhibits further adsorption of DEZ. The reduction of CuO is possible by the reactions of DEZ to form ZnO as described in Reactions 1–6. Figure 2b shows the XPS spectra of Zn-2p core levels after only DEZ molecules were introduced to the Cu_2O film at 90 °C. The Zn peak at 1021.6 eV (Zn-$2p_{3/2}$) corresponds to the peak of a reference ALD ZnO film grown by DEZ and H_2O_2. The thickness of the ZnO layer formed after the DEZ pulse to the Cu_2O film is estimated to be about 1 nm thick. Based on these observations, we conclude that starting the a-ZTO ALD process with the DEZ sequence is more effective to reduce the CuO surface layer than the process starting with the Sn(II) precursor sequence.

Although both reduction reactions to Cu_2O and metallic Cu are thermodynamically possible, metallic Cu is not detected after the metal precursor injections. It is difficult to distinguish Cu^{1+} from metallic Cu by XPS, because the peak positions of Cu-2p from the both states are close.[22] Instead, Cu_2O and Cu metal can be distinguished from the Cu-LMM Auger transition kinetic energy.[24] The Cu-LMM kinetic energies from Cu_2O and metallic Cu have been reported to be 916.5 and 918.4 eV, respectively, with Al-Kα radiation when the peaks were referenced to the C-1s binding energy at 284.6 eV.[24] As shown in Figure 2c, a kinetic energy of 916.9 eV is observed when the CuO phase was reduced by DEZ during the a-ZTO ALD process. Both the peak position and shape are closer to the signal from Cu_2O than from metallic Cu. To compare with the signal from the metallic Cu phase, a 20-nm-thick metallic Cu film was deposited by e-beam evaporation at room temperature and an a-ZTO film was grown on the Cu film. Obviously, the metallic Cu is observed at 919 eV, as well as a peak from the Cu_2O phase (formed by air exposure of Cu film after the growth) at 917 eV. The metallic Cu phase was detected successfully by XPS in the a-ZTO/Cu sample, owing to the a-ZTO layer protecting the Cu surface from the further oxidation by air. However, no metallic Cu phase was observed in the a-ZTO/Cu_2O sample. This indicates the formation of Cu may be limited kinetically

© 2014 WILEY-VCH Verlag GmbH & Co. KGaA, Weinheim

ADVANCED ENERGY MATERIALS
www.advenergymat.de

Materials Views
www.MaterialsViews.com

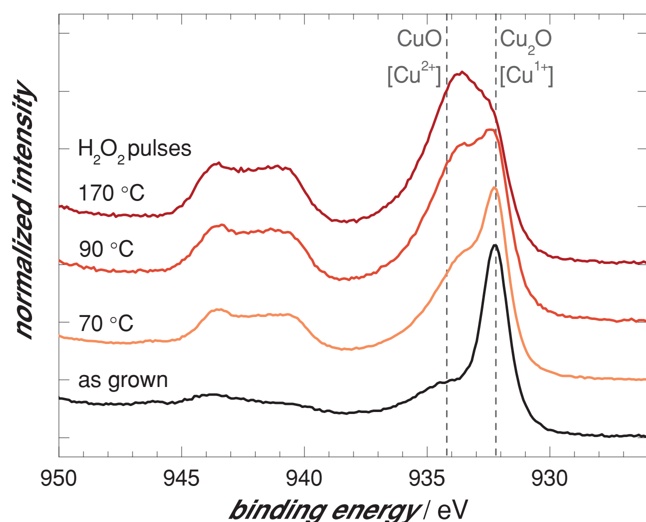

Figure 3. H_2O_2 exposure can re-oxidize the Cu_2O surface layer to CuO. Shown are normalized XPS spectra of Cu-2p for three different Cu_2O films. Only H_2O_2 pulses were injected on Cu_2O samples at reaction temperatures of 70, 90 and 170 °C.

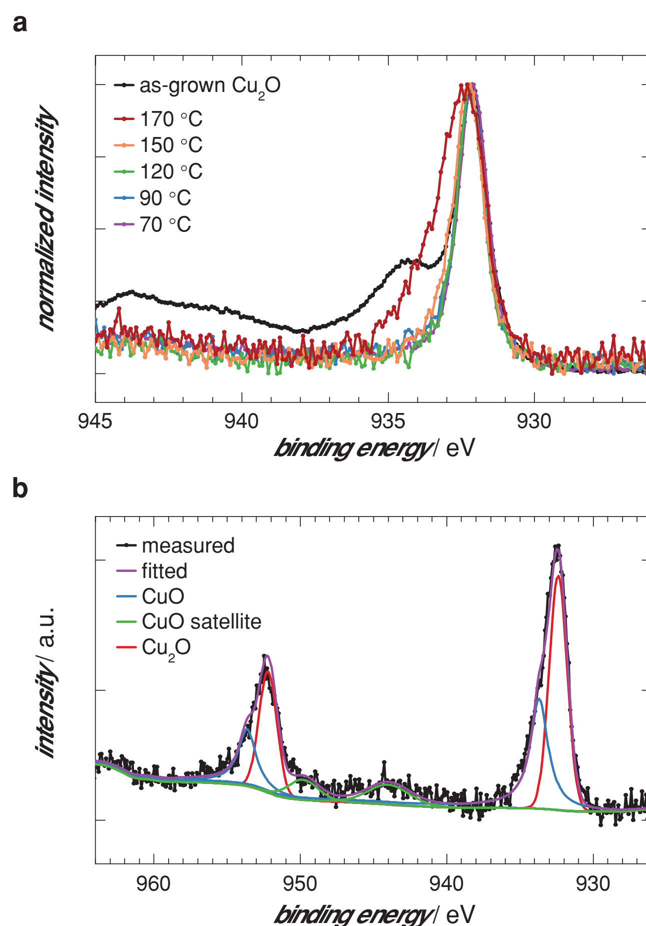

Figure 4. ALD reaction temperature can control the oxidation state of the Cu_2O surface layer. a) Normalized XPS spectra of Cu-2p from the Cu_2O samples after the growth of a-ZTO films at reaction temperatures between 70 and 170 °C. b) The deconvoluted XPS spectra of Cu-2p of Cu_2O surface with a-ZTO film grown at 170 °C, showing a peak shoulder at ≈933.7 eV corresponding to the Cu^{2+} state.

at the a-ZTO/Cu_2O sample, although the thermodynamic criteria for the formation of Cu are satisfied according to the Reactions 4–6. In addition, we investigated the potential for Cu diffusion through a-ZTO layers, since any trace of metallic Cu is known to pose significant diffusion issues as experienced in Cu-related processes of various semiconductor applications.[29] 10-nm-thick a-ZTO films, thicker than an electron escape depth of ≈5 nm in XPS, were deposited on Cu_2O at reaction temperatures between 90 and 170 °C. No signal from Cu is detected by XPS for all temperatures shown in Figure 2d. The Auger signal and the Cu-diffusion investigation did not indicate any trace of metallic Cu, which suggests that Reactions 4–6 are limited by high activation energies (slow kinetics).

On the other hand, H_2O_2 exposure after the DEZ sequence can re-oxidize the Cu_2O surface layer to the CuO phase. **Figure 3** shows the normalized XPS spectra of Cu-2p for three different Cu_2O samples: an as-grown Cu_2O film and H_2O_2-exposed Cu_2O films deposited at reaction temperatures of 70, 90 and 170 °C. Here, 36 H_2O_2 pulses were introduced to the Cu_2O samples, which is equal to the total H_2O_2 pulses of nine super-cycles. The increased satellite peak intensities at 940–945 eV for both temperatures indicate that the surface of the Cu_2O film is partly re-oxidized to CuO by H_2O_2. As the reaction temperature is raised from 70 to 170 °C, the intensity of the Cu^{2+} peak at 934 eV is increased relative to the Cu^{1+} peak at 932 eV. This result suggests that more oxidation of Cu_2O to CuO occurs at higher ALD temperatures.

Since the reduction and oxidation reactions possess different temperature dependences, the surface chemistry of Cu_2O films can be controlled by changing the reaction temperature. To investigate the chemical state of Cu at the a-ZTO/Cu_2O interface by XPS, 3-nm-thick a-ZTO films were grown on Cu_2O films at different reaction temperatures in the range of 70–170 °C. **Figure 4**a shows the normalized XPS spectra of Cu-2p from the a-ZTO/Cu_2O samples. The Cu^{2+} peak at 934 eV is not detected in samples with ALD reaction temperatures below 120 °C. This result suggests that the a-ZTO ALD process itself can effectively reduce the detrimental CuO layer to Cu_2O. However, at the reaction temperature of 170 °C, a small peak shoulder near ≈934 eV is observed. The peak shoulder is further investigated by deconvoluting the spectrum into multiple peaks as shown in Figure 4b. The peak shoulder is attributed to the Cu^{2+} state centering at ≈933.7 eV. As discussed in the previous experiments, a higher reaction temperature could increase the oxidation rate by H_2O_2 significantly, while the reduction rate by DEZ was not affected in the temperature range between 90 and 170 °C.

Thus, it can be concluded that the oxidation reaction by H_2O_2 competes with the reduction reaction by DEZ in the a-ZTO ALD process. As the reaction temperature increases, the oxidation reaction becomes faster than the reduction reaction, possibly due to different activation energies. It should be noted that the CuO formation by H_2O_2 is likely diffusion-limited by the a-ZTO layer: the oxidation by H_2O_2 becomes weaker as the a-ZTO layer gets thicker; thus the a-ZTO layer appears to protect the Cu_2O layer from further oxidation by H_2O_2. The Cu^{2+}

 © 2014 WILEY-VCH Verlag GmbH & Co. KGaA, Weinheim

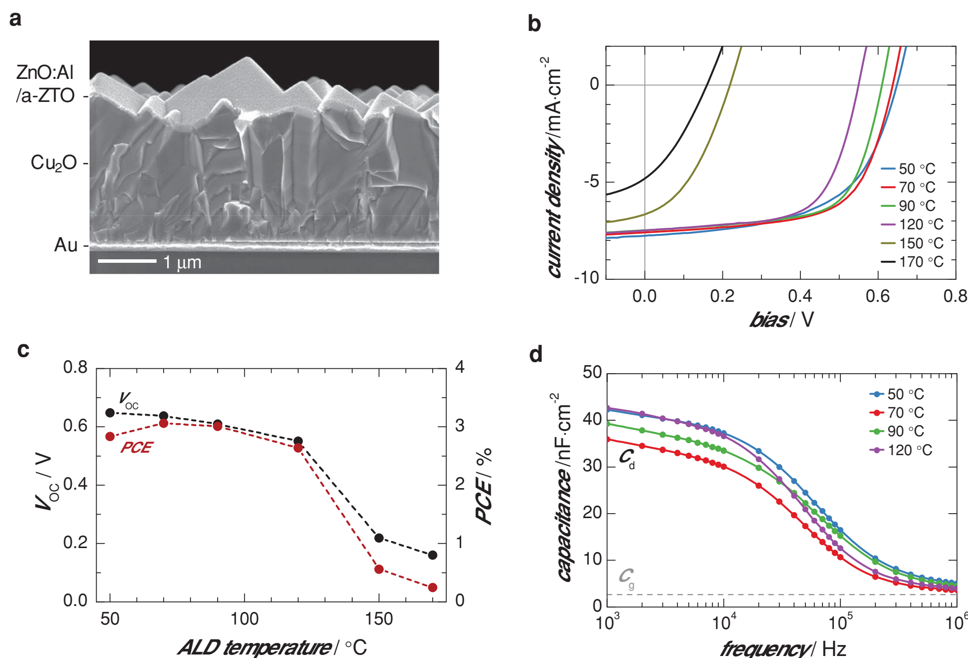

Figure 5. Characteristics of solar cell devices with varying Cu oxidation state at the Cu_2O/a-ZTO interface controlled by ALD temperature. a) A cross-sectional SEM image of Cu_2O-based solar cells with the device structure (ZnO:Al/a-ZTO/Cu_2O/Au). b) *J–V* characteristics of the devices under 1-sun (AM 1.5G) illuminated conditions. c) A summary of V_{OC} and PCE of the devices as a function of the a-ZTO ALD temperature. d) *C–f* characteristics of solar cell devices at room temperature with 0 mV and 10 mV for DC and AC bias, with a-ZTO films at reaction temperatures between 50 and 120 °C.

peak intensities relative to Cu^{1+} shown in Figure 4b are much smaller than ones where only H_2O_2 was injected, as shown in Figure 3. The protection of the substrate surface from the oxygen precursor by growing layers has also been proposed in other ALD processes.[27,30] Our XPS results suggest that a lower reaction temperature for a-ZTO ALD is beneficial for reducing the CuO surface layer to Cu_2O and preventing further re-oxidation by H_2O_2.

To demonstrate the effect of the interface chemistry control on solar cell performance, we fabricated Cu_2O-based solar cells with a-ZTO ALD reaction temperatures at 50–170 °C. **Figure 5**a shows a cross-sectional scanning electron microscopy (SEM) image of the device structure: ZnO:Al TCO (80 nm)/a-ZTO buffer (10 nm)/Cu_2O absorber (2.5 µm)/Au bottom electrode (200 nm). The ZnO:Al TCO layer was deposited in situ at 120 °C after the formation of the a-ZTO buffer layer on electrochemically-deposited Cu_2O. Here, the first ALD reaction of the a-ZTO buffer layer started with the injection of DEZ as discussed. Except for the ALD temperature of the a-ZTO buffer layer growth, all processing parameters were identical for all devices. Devices made at a-ZTO ALD temperatures of 150 and 170 °C showed slightly darker color than the other devices, possibly due to a CuO layer formed on the Cu_2O surface. The devices were completed by coating Al top-electrodes (1 µm) and MgF_2 anti-reflective layers (95 nm).

As the analysis of ALD reactions predicted, decreasing the ALD temperature enhances the solar-cell device performance. Current-density vs. voltage (*J–V*) characteristics of the devices were measured under 1-sun (AM 1.5G, 100 mW cm^{-2}) illumination conditions as shown in Figure 5b. While the short-circuit current densities (J_{SC}) remain between 7 and 8 mA cm^{-2}, the V_{OC} shows a strong dependence on the a-ZTO ALD temperature. The changes of V_{OC} and PCE of the devices are summarized as a function of the a-ZTO ALD temperature in Figure 5c. By decreasing the ALD temperature down to 50 °C, V_{OC} increases up to 0.65 V. However, the devices with ALD temperatures over 150 °C show a significant reduction of V_{OC} below 0.3 V. This drastic change can be explained by the increase of CuO content at higher ALD temperatures, increasing defect density at the a-ZTO/Cu_2O interface. The highest PCE of 3.06% is achieved with an a-ZTO ALD temperature of 70 °C. The device with an ALD temperature of 50 °C shows the highest V_{OC}, but its reduced fill-factor results in a lower PCE.

The possibility of bulk Cu_2O thermal degradation was ruled out by an additional experiment. A heat treatment of a Cu_2O layer at 150 °C before a-ZTO deposition at 70 °C was performed. The heat-treated device showed performance comparable to the device made without the heat treatment (Figure S2, Supporting Information), suggesting that the high temperature during a-ZTO deposition degrades only the heterojunction interface.

The heterojunction quality of the fabricated devices is further investigated by measuring capacitance vs. frequency (*C–f*) characteristics as shown in Figure 5d. A direct-current bias of 0 mV and an alternating-current bias of 10 mV were applied at room temperature. At high frequencies near 1 MHz, all devices show capacitances converging to 3–5 nF cm^{-2}, which is close to a simple geometric capacitance ($C_g \approx 2.7$ nF cm^{-2}) due to dielectric freeze-out. At low frequencies, on the other hand, the capacitances plateau to a depletion capacitance (C_d), which is dominated by the energy levels and densities of interfacial and bulk defects in the depleted region.[31] As the ALD temperature

© 2014 WILEY-VCH Verlag GmbH & Co. KGaA, Weinheim

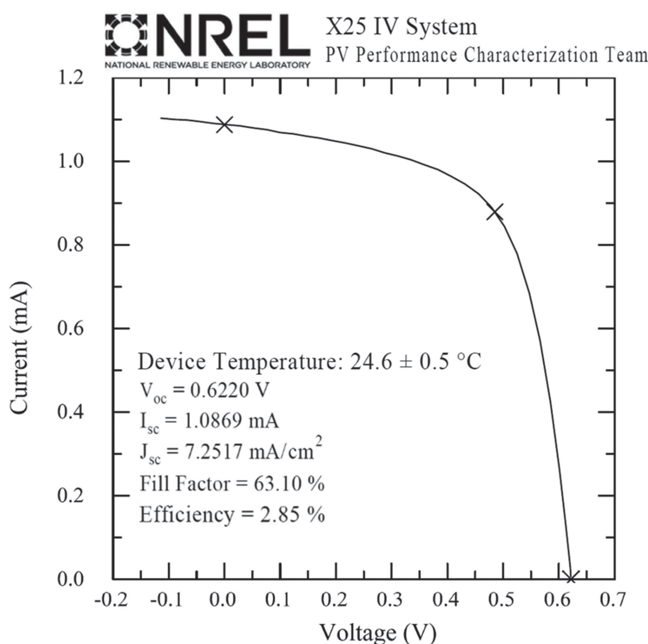

Figure 6. NREL certified *J–V* characteristics of the best device, with an a-ZTO buffer layer grown at 70 °C, under 1-sun (ASTM G173 global) illumination.

for a-ZTO decreases from 120 to 70 °C, the capacitance at 1 kHz decreases from 42.7 to 35.9 nF cm^{-2}, which suggests reduced Cu^{2+}-related defect densities at the a-ZTO/Cu_2O interface. However, the ALD temperature of 50 °C shows a higher capacitance than that of 70 °C, possibly due to bulk defects in the a-ZTO layer. Too-low ALD reaction temperature often results in increased carbon and nitrogen-related impurities, which might be mitigated with plasma-assisted ALD.[32,33]

The device with the highest efficiency was characterized independently at the National Renewable Energy Laboratory (NREL). The *J–V* characteristic of the device under the ASTM G173 global 1-sun illumination is shown in **Figure 6**. The device was measured on a temperature-controlled stage, after a 10-minute light-soak at the maximum power condition (a forward bias of 0.49 V) and a 5-min cool down. A spectral mismatch correction was applied using a normalized quantum efficiency (QE) spectrum (Figure S3, Supporting Information) to measure accurate device performance. The device shows a PCE of 2.85%. The V_{OC}, J_{SC}, and fill-factor of the device are 622 mV, 7.25 mA cm^{-2}, and 63.1%, respectively. A small discrepancy from the result shown in Figure 5 is observed, which could be from a spectral mismatch of the light source and a different device temperature during the measurements. The measurement at NREL is the first verified efficiency of Cu_2O-based thin-film solar cells measured independently to date.

In summary, the presence of a deleterious CuO layer at the a-ZTO/Cu_2O interface can be minimized by optimizing the a-ZTO ALD process to reduce this layer to Cu_2O, enhancing the heterojunction open-circuit voltage. In our Cu_2O thin films grown by electrochemical deposition, a nanometer-scale thick CuO surface layer is formed by air exposure. Starting the first ALD sequence with the highly reactive DEZ pulse effectively reduces the CuO surface layer to Cu_2O by forming ZnO. As the ALD temperature is increased, re-oxidation of Cu_2O to CuO by H_2O_2 becomes a dominant reaction over the reduction of CuO by DEZ. By engineering the Cu_2O surface chemistry with the a-ZTO ALD temperature, the chemical state of Cu at the interface can be controlled and the formation of a high-quality heterojunction is demonstrated. The controlled interface chemistry increases the V_{OC} of a-ZTO/Cu_2O solar cells, resulting in an independently verified PCE of 2.85%. This approach may also be useful in other material systems that employ ALD overlayers (buffer layers and TCOs), to improve interface quality by engineering cation chemical states locally at the interface.

Experimental Section

Atomic Layer Deposition of a-ZTO Thin Films: The a-ZTO thin-films were deposited using a custom-built cylindrical ALD reactor with a sample stage 30 cm long and 3 cm wide, and a chamber volume of 0.627 L. The aluminum substrate stage and the entire wall of ALD chamber were kept at the same ALD reaction temperature inside a Lindberg Blue M tube furnace (Thermo Scientific). Diethylzinc (Sigma Aldrich) and 1,3-bis(1,1-dimethylethyl)-4,5-dimethyl-(4R,5R)-1,3,2-diazastannolidin-2-ylidene were used as Zn and Sn precursors, respectively. The Zn and Sn precursors were kept at constant temperature of 25 and 40 °C, respectively. A H_2O_2 solution (50 wt% in H_2O, Sigma Aldrich) was used as a common oxidant for a-ZTO growth to enable the ALD reaction with the Sn(II) precursor at reaction temperature below 170 °C, which was not possible by using H_2O. Due to a high vapor pressure of H_2O_2, as-received H_2O_2 solution was placed in a glass container held at 25 °C and it was vaporized into a trap, which is made of stainless steel with a volume of 35 mL, prior to the release into the ALD reactor. One super-cycle of a-ZTO consisted of ZnO and SnO_2 sub-cycles with a ratio of 3:1. During the each sub-cycle, the exposures of diethylzinc, tin precursor, and H_2O_2 were estimated to be approximately 0.32, 0.033, and 0.027 Torr s, respectively. Further details on electrical, structural, and optical properties of a-ZTO films grown by ALD are described elsewhere.[9,25]

Solar Cell Fabrication: A 200-nm-thick Au bottom-electrode with 5-nm-thick Ti adhesion layer was deposited on a 1 × 1 inch^2 SiO_2 by e-beam evaporation. To define a cell area of 3 × 5 mm^2, a 2.5-μm-thick SiO_2 layer was deposited by plasma-enhanced chemical vapor deposition and areas defined by photolithography were etched by a buffered-oxide-etchant (7:1, J. T. Baker). A 2.5-μm-thick Cu_2O film was deposited on the exposed Au area at 40 °C by the galvanostatic electrochemical method.[9,34,35] A lactate-stabilized copper sulfate aqueous solution was prepared with 3 M lactic acid (Sigma Aldrich), 0.2 M cupric sulfate pentahydrate ($CuO_4{\cdot}5H_2O$, Sigma Aldrich) and de-ionized water (18.3 MΩ cm, Ricca Chemical), and then 2 M sodium hydroxide (NaOH, Sigma Aldrich) aqueous solution was added to adjust the pH of the solution to 12.5. All reagent-grade chemicals were used and the solution was filtered and stirred thoroughly. A constant current density of 0.23 mA cm^{-2} was applied for 2 h using a Keithley 2400 sourcemeter with a Pt counter electrode to grow the Cu_2O films. The Cu_2O film surfaces were rinsed with de-ionized water. The a-ZTO and ZnO:Al thin-films were deposited by ALD as described in detail elsewhere.[9] 1-μm-thick Al top-electrodes were deposited by e-beam evaporation with a grid spacing of 0.5 mm defined by a lift-off process. A 95-nm-thick MgF_2 film as an antireflective layer was deposited by thermal evaporation.

Characterization: Surface morphologies of the devices were analyzed using an Ultra 55 FESEM (Zeiss). XPS measurements were performed using a K-alpha XPS (Thermo Scientific). Samples were etched in situ by an Ar ion beam for a depth profiling. The *J–V* and the *C–f* characteristics of the devices were measured by using Agilent 4156C and Keithley 2400 semiconductor characterization systems. The standard 1-sun illumination was generated by a Newport Oriel 91194 solar simulator with a 1600 W ozone-free Xe-lamp with a AM1.5G filter and a Newport

© 2014 WILEY-VCH Verlag GmbH & Co. KGaA, Weinheim

Oriel 6895 f1ux controller calibrated by an NREL-certified Si reference cell equipped with a BG-39 window.

Supporting Information

Supporting Information is available from the Wiley Online Library or from the author.

Acknowledgements

S.W.L. and Y.S.L. contributed equally to this work. The authors acknowledge scientific discussions with S.S. Wilson and H.A. Atwater (Caltech). The authors thank P. Ciszek and K. Emery (NREL) and their team for assistance with certified cell testing. This work was supported by the Office of Naval Research ONR N00014–10–1–0937, the National Science Foundation (NSF) award CBET-1032955, and NSF CAREER award ECCS-1150878. This work made use of the Center for Nanoscale Systems at Harvard University and the Microsystems Technology Laboratories at MIT supported by NSF awards ECS-0335765 and DMR-0819762, respectively. A Clean Energy Scholarship from NRF Singapore (S.C.S.) and an NSF Graduate Research Fellowship (R.E.B.) are acknowledged.

Received: December 13, 2013
Revised: February 25, 2014
Published online:

[1] R. W. Birkmire, E. Eser, *Annu. Rev. Mater. Sci.* **1997**, *27*, 625.
[2] W. Jaegermann, A. Klein, T. Mayer, *Adv. Mater.* **2009**, *21*, 4196.
[3] B. K. Meyer, A. Polity, D. Reppin, M. Becker, P. Hering, P. J. Klar, T. Sander, C. Reindl, J. Benz, M. Eickhoff, C. Heiliger, M. Heinemann, J. Bläsing, A. Krost, S. Shokovets, C. Müller, C. Ronning, *Phys. Status Solidi B* **2012**, *249*, 1487.
[4] K. P. Musselman, A. Wisnet, D. C. Iza, H. C. Hesse, C. Scheu, J. L. MacManus-Driscoll, L. Schmidt-Mende, *Adv. Mater.* **2010**, *22*, E254.
[5] C. Xiang, G. M. Kimball, R. L. Grimm, B. S. Brunschwig, H. A. Atwater, N. S. Lewis, *Energy Environ. Sci.* **2011**, *4*, 1311.
[6] S. Jeong, S. H. Song, K. Nagaich, S. A. Campbell, E. S. Aydil, *Thin Solid Films* **2011**, *519*, 6613.
[7] A. Mittiga, E. Salza, F. Sarto, M. Tucci, R. Vasanthi, *Appl. Phys. Lett.* **2006**, *88*, 163502.
[8] K. P. Musselman, A. Marin, A. Wisnet, C. Scheu, J. L. MacManus-Driscoll, L. Schmidt-Mende, *Adv. Funct. Mater.* **2011**, *21*, 573.
[9] Y. S. Lee, J. Heo, S. C. Siah, J. P. Mailoa, R. E. Brandt, S. B. Kim, R. G. Gordon, T. Buonassisi, *Energy Environ. Sci.* **2013**, *6*, 2112.
[10] T. Minami, Y. Nishi, T. Miyata, *Appl. Phys. Express* **2013**, *6*, 044101.
[11] T. S. Gershon, A. K. Sigdel, A. T. Marin, M. F. A. M. van Hest, D. S. Ginley, R. H. Friend, J. L. MacManus-Driscoll, J. J. Berry, *Thin Solid Films* **2013**, *536*, 280.
[12] M. T. Greiner, M. G. Helander, W. M. Tang, Z. B. Wang, J. Qiu, Z. H. Lu, *Nat. Mater.* **2012**, *11*, 76.
[13] F. P. Koffyberg, F. A. Benko, *J. Appl. Phys.* **1982**, *53*, 1173.
[14] S. S. Wilson, Y. Tolstova, H. A. Atwater, *IEEE Photovoltaic Spec. Conf., 39th*, DOI: 10.1109/PVSC.2013.6744960.
[15] J.-W. Lim, J. Iijima, Y. Zhu, J. H. Yoo, G.-S. Choi, K. Mimura, M. Isshiki, *Thin Solid Films* **2008**, *516*, 4040.
[16] B. Canava, O. Roussel, J. F. Guillemoles, D. Lincot, A. Etcheberry, *Phys. Status Solidi C* **2006**, *3*, 2551.
[17] B. Canava, J. Vigneron, A. Etcheberry, J. F. Guillemoles, D. Lincot, *Appl. Surf. Sci.* **2002**, *202*, 8.
[18] Y. Nishi, T. Miyata, J.-I. Nomoto, T. Minami, *Thin Solid Films* **2012**, *520*, 3819.
[19] J. R. Bakke, K. L. Pickrahn, T. P. Brennan, S. F. Bent, *Nanoscale* **2011**, *3*, 3482.
[20] J. A. van Delft, D. Garcia-Alonso, W. M. M. Kessels, *Semicond. Sci. Technol.* **2012**, *27*, 074002.
[21] P. Poodt, A. Lankhorst, F. Roozeboom, K. Spee, D. Maas, A. Vermeer, *Adv. Mater.* **2010**, *22*, 3564.
[22] J. C. Klein, A. Proctor, D. M. Hercules, J. F. Black, *Anal. Chem.* **1983**, *55*, 2055.
[23] J. Ghijsen, L. H. Tjeng, J. van Elp, H. Eskes, J. Westerink, G. A. Sawatzky, M. T. Czyzyk, *Phys. Rev. B* **1988**, *38*, 11322.
[24] S. Poulston, P. M. Parlett, P. Stone, M. Bowker, *Surf. Interface Anal.* **1996**, *24*, 811.
[25] J. Heo, S. B. Kim, R. G. Gordon, *Appl. Phys. Lett.* **2012**, *101*, 113507.
[26] S. W. Lee, J. H. Han, S. K. Kim, S. Han, W. Lee, C. S. Hwang, *Chem. Mater.* **2011**, *23*, 976.
[27] S. W. Lee, Y. Liu, J. Heo, R. G. Gordon, *Nano Lett.* **2012**, *12*, 4775.
[28] *The Gibbs free energies of reactions were calculated from the Gibbs free energy data of each chemical species from the library of HSC Chemistry software* 5.11 edition, Outokumpu Research Oy, Pori, Finland, **2002**.
[29] Z. Li, R. G. Gordon, D. B. Farmer, Y. Lin, J. Vlassak, *Electrochem. Solid-State Lett.* **2005**, *8*, G182.
[30] S. W. Lee, J. Heo, R. G. Gordon, *Nanoscale* **2013**, *5*, 8940.
[31] T. Walter, R. Herberholz, C. Müller, H. W. Schock, *J. Appl. Phys.* **1996**, *80*, 4411.
[32] J. Fan, H. Liu, Q. Kuang, B. Gao, F. Ma, Y. Hao, *Microelectron. Reliab.* **2012**, *52*, 1043.
[33] S. T. Lehti, *Eur. Phys. J. D* **2013**, *67*, 82-1.
[34] Y. S. Lee, J. Heo, M. T. Winkler, S. C. Siah, S. B. Kim, R. G. Gordon, T. Buonassisi, *J. Mater. Chem. A* **2013**, *1*, 15416.
[35] P. E. de Jongh, D. Vanmaekelbergh, J. J. Kelly, *Chem. Mater.* **1999**, *11*, 3512.

© 2014 WILEY-VCH Verlag GmbH & Co. KGaA, Weinheim